

# Stiffness-guided motion of a droplet on a solid substrate

Panagiotis E. Theodorakis\*

*Institute of Physics, Polish Academy of Sciences, Al. Lotników 32/46, 02-668 Warsaw, Poland*

Sergei E. Egorov†

*Department of Chemistry, University of Virginia, Charlottesville, VA 22901, USA*

*Institut für Physik, Johannes Gutenberg Universität Mainz, 55099 Mainz, Germany and*

*Leibniz-Institut für Polymerforschung, Institut Theorie der Polymere, Hohe Str. 6, 01069 Dresden, Germany*

Andrey Milchev‡

*Bulgarian Academy of Sciences, Institute of Physical Chemistry, 1113 Sofia, Bulgaria*

(Dated: June 30, 2021)

A range of technologies require the directed motion of nanoscale droplets on solid substrates. A way of realizing this effect is durotaxis, whereby a stiffness gradient of a substrate can induce directional motion without requiring an energy source. Here, we report on the results of extensive molecular dynamics investigations of droplets on a surface with varying stiffness. We find that durotaxis is enhanced by increasing the stiffness gradient and, also, by increased wettability of the substrate, in particular, when droplet size decreases. We anticipate that our study will provide further insights into the mechanisms of nanoscale directional motion.

Keywords: Molecular dynamics simulations, durotaxis, wetting

## I. INTRODUCTION

A range of technologies require the control of liquids on surfaces, such as microfabrication [1] and coating [2, 3] with many of these applications also requiring a directed motion of nanodroplets onto the surface [2, 4–6]. To this end, many methods have been explored, for example heterogeneous surface chemistries for different patterns [7–9], temperature and electric potential gradients [2, 6], and surface topography [10–14]. Other techniques for moving nanoscale objects are based on electrical current [15–18], charge [19–21], thermal energy (selective heating) [22–24], simple stretch [25], and complicated chemical reactions (e.g. in biological processes) [26]. In the context of biology, directional motion of cells takes place due to various stimuli, such as substrate chemicals, light, gravity and electrostatic potential [27]. Recent studies have shown that cell movements are also guided by substrate stiffness (rigidity), a phenomenon known as durotaxis [28].

Inspired by durotaxis in biology, solid substrate durotaxis has emerged as an attractive research field as the motion of nanoscale objects can be guided by substrate stiffness without the requirement for an energy source with implications for nanoscale actuation and energy conversion [29–33]. Moreover, solid substrate durotaxis, which was investigated by using computer simulation in the context of a flake sliding on a graphene substrate with a stiffness gradient, shares similarities with the stiffness-guided directional motion in living cells as in

both cases weak van der Waals interactions are present [30]. In particular, the interaction between the substrate and the flake was inversely proportional to the stiffness [30]. Lower potential energies are more stable than higher ones, and this explains the motion towards the higher stiffness adopting a thermodynamically favorable state [33, 34]. In this case, computer simulation has been an extremely useful tool to interpret the modeled process, as materials were electrically, chemically and thermally isolated free of defects and impurities. Here, we study durotaxis in the context of a liquid droplet on a solid substrate with a stiffness gradient by means of computer simulation. In particular, we explore different stiffness gradients, droplet sizes, and levels of attraction between the droplet and the substrate. Our results highlight the importance of interfacial energy between the droplet and the substrate, in agreement with Chang *et al.* [30]. We anticipate that our study will provide further insights into substrate patterning leading to new opportunities in nanoscale science and technology [34].

## II. THE MODEL

In this study we consider a system comprised of a liquid droplet on a substrate with stiffness gradient. The droplet consists of  $N_p$  polymer chains ( $N_p = 100, 600, \text{ or } 4800$ ) with  $N = 10$  segments each. For the chosen chain length the vapor pressure is sufficiently low and evaporation effects are negligible [12]. Owing to the comparatively small size of the droplets, important quantities that characterize the droplet, such as the contact angle, are subject to strong fluctuations, while in addition such properties become also size dependent [35].

The substrate is formed by a layer of spherical beads,

---

\*Electronic address: panos@ifpan.edu.pl.

†Electronic address: sae6z@eservices.virginia.edu.

‡Electronic address: milchev@ipc.bas.bg

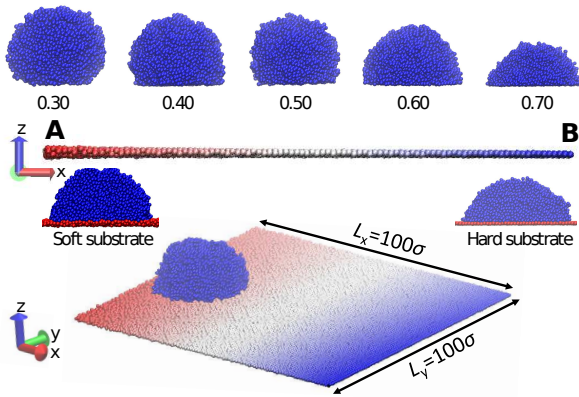


FIG. 1: Upper panel illustrates the shape of the droplet on a stiff substrate for different strength of attraction ( $\varepsilon_{sp} = 0.30 \dots 0.70$ ) as indicated. Middle panel shows the effect of the substrate stiffness gradient in  $x$ -direction, marked by red color (left side of the substrate, A) for soft substrate, and by blue color (on the B-side of the substrate in  $x$ -direction) indicating the highest rigidity. Two examples of droplets “sitting” on soft and stiff substrates for the case  $\varepsilon_{sp} = 0.70$  are also shown. In the bottom panel we denote by color gradient the change in the degree of stiffness every  $\Delta L = 4\sigma$  in the  $x$ -direction. Snapshots were taken by using the VMD software [36].

positioned on a square lattice with lattice constant  $\alpha$ , where  $\alpha = \sigma$ , with bead diameter  $\sigma$  serving here also as a unit of length. The substrate is chosen with linear dimensions in the  $x$  and  $y$  directions  $L_x = L_y = 100\sigma$ , respectively (see Fig. 1).

Interactions between different components of the system, i.e., drop particles and substrate beads, are described by means of the Lennard-Jones potential, i.e.,

$$U_{LJ}(r) = 4\varepsilon_{ij} \left[ \left( \frac{\sigma_{ij}}{r} \right)^{12} - \left( \frac{\sigma_{ij}}{r} \right)^6 \right], \quad (1)$$

where  $r$  is the distance between any pair of beads in the system, and  $i$  and  $j$  indicate the type of beads: “ $p$ ” stands for polymer beads, and “ $s$ ” denotes substrate beads. In the present consideration,  $\sigma_{pp} = \sigma_{ss} = \sigma_{sp} = \sigma$ . As usual, the LJ-potential is cut and shifted at a cutoff distance  $r_c = 2.5\sigma$  for the “ $pp$ ” and “ $sp$ ” interactions, while for the interaction between substrate beads  $r_c = 2^{1/6}\sigma$  (i.e., a purely repulsive interaction). The parameter  $\varepsilon_{ij}$  of the LJ potential for the polymer and the substrate is  $\varepsilon_{pp} = \varepsilon_{ss} = \varepsilon$ , while  $\varepsilon_{sp}$  was used to tune the affinity between the substrate and the droplet. Here,  $\varepsilon_{sp} = 0.3, 0.4, 0.5, 0.6,$  and  $0.7$  in units of  $\varepsilon$ . For example, the choice of  $\varepsilon_{sp} = 0.5$  provides a droplet contact-angle  $\theta$  of roughly  $90^\circ$  on stiff substrates, which, of course, is size and model dependent [35].

The finite extensible nonlinear elastic (FENE) potential [37] was used to keep together consecutive beads in

the polymer chain. The FENE potential reads

$$U_{FENE}(r) = -0.5K_{FENE}R_0^2 \ln \left[ 1 - \left( \frac{r}{R_0} \right)^2 \right], \quad (2)$$

where  $r$  is the distance between two consecutive bonded beads along the polymer backbone,  $R_0 = 1.5\sigma$  expresses the maximum extension of the bond, and  $K_{FENE} = 30\varepsilon/\sigma^2$  is an elastic constant.

Substrate beads are tethered to their lattice sites by a harmonic potential with spring constant  $K$  (the factor  $1/2$  is absorbed in the constant), which is used as a parameter for tuning the substrate stiffness. Small values of  $K$  result in large fluctuations of the substrate beads around their position on the lattice sites, which corresponds to small substrate stiffness (soft substrates), whereas large values of  $K$  result in strong tethering of the substrate beads to their lattice sites resulting in a large stiffness (hard substrate) [9]. The stiffness gradient is implemented along the  $x$ -direction (see Fig. 1): Starting from an initial stiffness  $K_0$ , (expressed in units  $\varepsilon/\sigma^2$  with  $\varepsilon$  being the unit of energy) at the very left side (point A in Fig. 1) of the substrate with coordinate  $x = 0$ , we increase the stiffness by  $\Delta K$  every  $\Delta L = 4\sigma$  until the right end of the substrate (point B in Fig. 1) in the  $x$ -direction with stiffness  $K_f$  is reached. Hence, the stiffness for each bead depends on the set  $(K_0, \Delta K)$ , according to the relation  $K = K_0 + n * \Delta K$ , where  $n$  is an integer that indicates the number of times we increased the stiffness in the  $x$  direction by an amount  $\Delta K$  every  $\Delta L = 4\sigma$ . In our study, we explore different sets of these parameters along with the adhesion parameter  $\varepsilon_{sp}$  studying droplets of different size  $N_p$ .

To evolve our system in time, we used Molecular Dynamics (MD) simulations by choosing the Langevin thermostat [38] as implemented in the LAMMPS package [39]. The time unit in our simulations is  $\tau = \sqrt{m\sigma^2/\varepsilon}$ , where  $m \equiv 1$  is the mass unit of the drop particles and the substrate beads. The integration time-step for the velocity-Verlet integration of the equations of motion is  $\Delta t = 0.005\tau$ . Thus, the temperature  $T$  fluctuates around a predefined value  $T = \varepsilon/k_B$ , where  $k_B$  is the Boltzmann constant, and the energy  $\varepsilon$  is measured in units of  $k_B T$ . The total number of beads of the system is fixed and the total volume of the system, which is also constant, corresponds to the size of the simulation box, that is,  $L_x \times L_y \times L_z$  with  $L_z$  large enough so as to guarantee that neither the substrate nor the polymer droplet interact with their periodic images in the  $z$ -direction. Typical trajectories start at the left edge of the droplet positioned at point A of the substrate (see Fig. 1) while the simulations run up to  $10^8$  MD time steps. Our results are based on the analysis of ten independent trajectories for each set of values  $(K_0, \Delta K, \varepsilon_{sp}, \text{ and } N_p)$ .

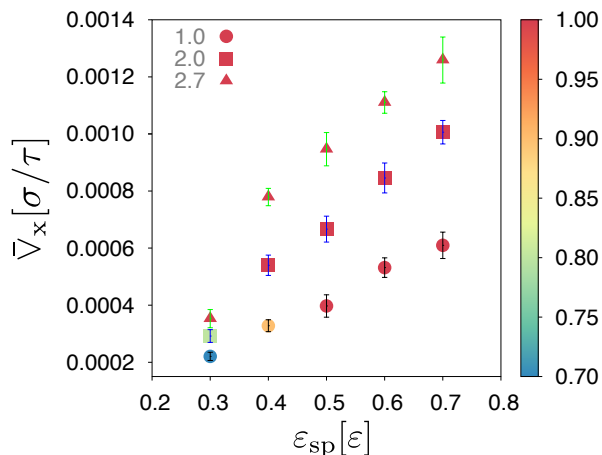


FIG. 2: The mean velocity  $\bar{v}_x$  by which the droplet moves from A to B (cf. Fig. 1; the center of mass of the droplet is taken into account to estimate the distance) versus the attraction of the droplet to the substrate  $\epsilon_{sp}$  for different values of the gradient  $dK/dx$  as indicated. The color bar indicates the probability that the droplet will cover the distance from A to B within the simulation time ( $10^8$  MD steps). The droplet is formed by  $N_p = 600$  chains.

### III. RESULTS

We have studied three different substrates with the *same* average stiffness in order to examine the role of the stiffness gradient in durotaxis (see Fig. 2). If the stiffness at the right most end of the substrate ( $B$  in Fig. 1) is  $K_f$ , then the mean stiffness will be  $K_{ave} = (K_0 + K_f)/2$  for substrates with constant gradient along the  $x$ -direction. Here, we set  $K_{ave} = 148\epsilon/\sigma^2$ , and the three chosen sets of  $(K_0, \Delta K)$  are  $(20, 10.666)$ ,  $(50, 8.166)$ , and  $(100, 4)$ , corresponding to values of the gradient,  $K' \equiv dK/dx = 2.7, 2.0$ , and  $1.0$ , respectively. The degree of droplet adhesion to the substrate, governed by the droplet–substrate affinity  $\epsilon_{sp}$  also affects the process of durotaxis, and should be taken into account by varying the strength of  $\epsilon_{sp}$ . With this choice of parameters, the droplet is found to perform a predominantly translational movement from the soft edge towards the rigid end of the substrate. In Fig. 2 we plot the observed mean velocity  $\bar{v}_x$ , averaged over ten individual droplets, as function of the surface adhesion  $\epsilon_{sp}$  for the three rigidity gradients  $K'$ .

One should note, however, that drops, depending on the concrete values of the aforementioned parameters, undergo partially random displacements away from the gradient  $x$ -direction, so that not all droplets manage to reach the stiff edge of the substrate within the time window of the computer experiment. Therefore, in Fig. 2 we use a color bar to indicate the share of droplets that successfully traverse the distance between the soft and the stiff edge of the substrate.

Apparently, the results, displayed on Fig. 2 indicate, that the mean velocity of drops,  $\bar{v}_x$ , on three substrates

with the *same* average stiffness, increases steadily and proportionally to the magnitude of the stiffness gradient  $K'$ . In addition, the higher attraction between the droplet and the substrate leads to larger mean velocity of the droplet during durotaxis irrespective of the magnitude of the stiffness gradient. Moreover, the probability of durotaxis is lower than one in the case of small gradients and weak adhesion  $\epsilon_{sp}$ . These findings represent the central results of this investigation. A plot of our simulation data, cf. Fig. 3, as a function of the gradient,  $K'$ , for different strength of adhesion,  $\epsilon_{sp}$ , and comparison with Fig. 2 indicates that the mean speed of durotaxis changes linearly with the stiffness gradient,  $K'$ ,

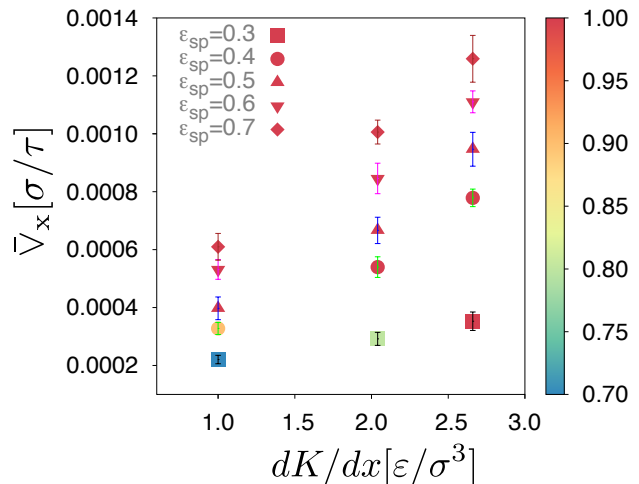


FIG. 3: The mean velocity  $\bar{v}_x$  (similarly to 2) versus the gradient  $dK/dx$  for various levels of attraction between the droplet and the substrate, as indicated. The color bar indicates the probability of durotaxis within the simulation time ( $10^8$  MD steps). The droplet is formed by  $N_p = 600$  chains.

and with the strength of attraction between the droplet and the substrate,  $\epsilon_{sp}$ , namely, droplets move faster on better wettable substrates. Therefore, our parameter exploration for various cases, suggests that higher stiffness gradient and stronger affinity between the droplet and the substrate result in more efficient durotaxis.

As is well known, the size of small (nano)droplets affects the resulting contact angle and the degree of droplet adhesion on surfaces whenever the free energy of the contact line becomes comparable to the surface free energy (surface tension). One may, therefore, expect that durotaxis will also depend on droplet size [40]. We have investigated different drop sizes (see Fig. 4) and we established that the bigger the droplet is, the less efficient durotaxis becomes. Our observation holds for the whole range of  $\epsilon_{sp}$  values considered in this study. In particular, the smallest droplet with ( $N_p = 100$ ) exhibits the fastest durotaxis reaching a threshold speed value when  $\epsilon_{sp} > 0.5$ , whereas the largest droplet ( $N_p = 4800$ ) exhibits a linear dependence with the parameter  $\epsilon_{sp}$ . We interpret this result as consequence of the increased friction due to the larger area of contact with the substrate

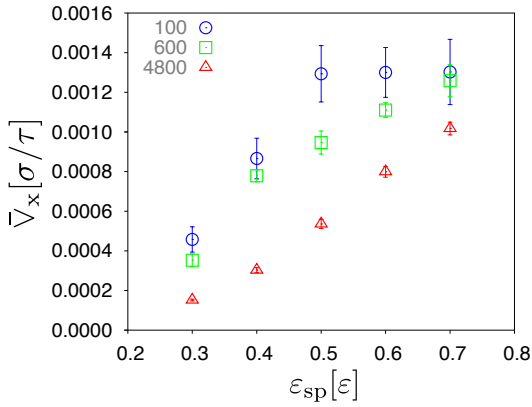


FIG. 4: The mean velocity  $\bar{V}_x$  versus the parameter  $\varepsilon_{sp}$  that governs the adhesion to the substrate for droplets containing  $N_p = 100, 600,$  and  $4800$  polymer chains with ten monomers. Here at the soft edge of the substrate  $K_0 = 20$ , and the stiffness gradient  $K' = 2.7$ . For all different cases of droplet size, the probability of durotaxis is 100%

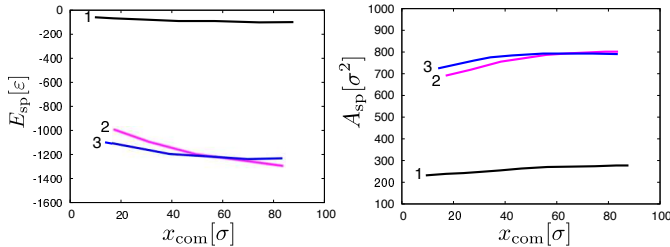


FIG. 5: Interaction energy between droplet and substrate,  $E_{sp}$  (left panel), and interfacial area,  $A_{sp}$  (right panel), as a function of the centre-of-mass-position (COM) of the droplet,  $x_{com}$ , for the cases  $K_0 = 20, K' = 2.7, \varepsilon_{sp} = 0.30$  (1),  $K_0 = 20, K' = 2.7, \varepsilon_{sp} = 0.70$  (2) and  $K_0 = 100, K' = 1.0, \varepsilon_{sp} = 0.70$  (3) for a drop with  $N_p = 600$ . In the case of optimal durotaxis, the droplet gains energy  $E_{sp}$  faster as it moves to stiffer parts of the substrate. In contrast, when this gain is negligible, no durotaxis takes place. Here, substrate and droplet beads within the cutoff distance  $2.5\sigma$  are considered as part of the interface. The interfacial area has been calculated by projecting the droplet beads of the interface onto the  $z=0$  layer and determining the convex hull by using the qhull library. [41] In this case the area of the convex hull is the interfacial area.

associated with the big droplet. One should also note that this observation is at variance with the results of Style *et al.* [29], who found that a drop moves spontaneously toward softer parts of the substrate, once the contact angle difference across the droplet,  $\Delta\theta$ , exceeds some critical value, given that  $\Delta\theta$  would be also larger for the bigger droplets. Our results comply, however, with those of Chang *et al.* [30] who used similar architecture of the substrate as ours, which makes us believe that the concrete implementation of varying degree of stiffness along the substrate largely determines the outcome of durotaxis.

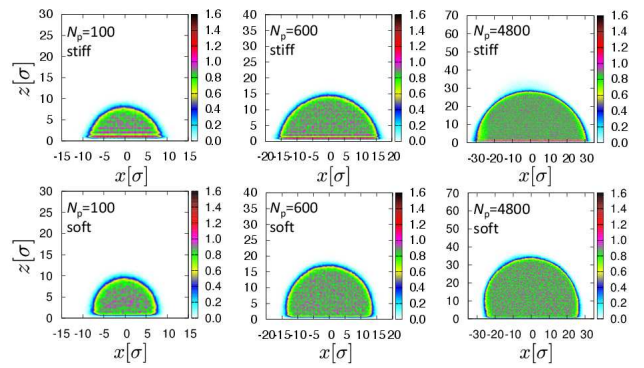


FIG. 6: The density profiles on the  $x - z$  plane for different droplet sizes and substrate stiffness is illustrated, as indicated. For soft substrate the stiffness is  $K = 276$ , whereas for the soft substrates is  $K = 20$ . The figure illustrates the dependence of the contact angle with the droplet size [35] and the substrate stiffness.

Based on our detailed analysis of a larger number of different properties and systems, the driving force for durotaxis on a substrate with variable stiffness stems from the possibility for the droplet to diminish its overall energy by displacement to stiffer regions on the substrate, in agreement with previous work in the context of a flake on a graphene layer [30, 33]. Fig. 5 illustrates examples of systems with different durotaxis efficiency. Comparing these results with those of Figures 2 and 3, we observe that larger variations in the interfacial energy  $E_{sp}$  with changing position  $x$  lead to more efficient durotaxis.

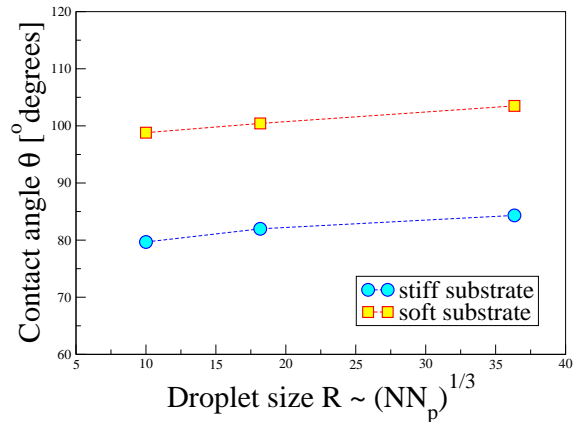


FIG. 7: Variation of the contact angle  $\theta$  of sessile drops, cf. Fig. 6, with drop radius  $R \propto (NN_p)^{1/3}$  on a soft,  $K = 20$ , and stiff,  $K = 276$ , substrates.

In this case, the droplet is able to establish a larger number of contacts with the substrate and get attracted stronger by the interface. This results in changes of many properties with the centre-of-mass displacement of the droplet, such as the radius of gyration of the droplet, the interfacial area between the droplet and the substrate,

as well as the contact angle  $\theta$ . Analyzing the various contributions to the total energy of the system, it appears that minimization of the interfacial energy  $E_{sp}$  (expressed through  $dE_{sp}/dx_{com}$ ) serves as the main driving force for efficient durotaxis.

Moreover, by exploring droplets of different size, and analyzing the respective density profiles, cf. Fig. 6), we find that larger droplets are generally more hydrophobic than smaller ones for the same values of  $\varepsilon_{sp}$  and degree of substrate stiffness. This indicates that as the drop size decreases, a gain from negative line tension compensates increasingly the energy expense related to the vapor-liquid surface of the drop [42] as established earlier by Gretz [43].

We also observe that the contact angle  $\theta$  for droplets of different size is always smaller at stiffer substrates (whereby the stronger attraction to the substrate leads to layering effects) than it is for soft substrates (Figs. 6 and 7). As is evident from Fig. 6, the droplet does not “immerse” into the softer part of the substrate, but rather, irrespective of the stiffness, the substrate is able to support the droplet. One may, therefore, conclude that the interfacial energy, which is the governing force of durotaxis, depends on the size of the droplet, the substrate stiffness, as well as on the substrate wettability, whereby stronger stiffness gradients enhance the durotaxis.

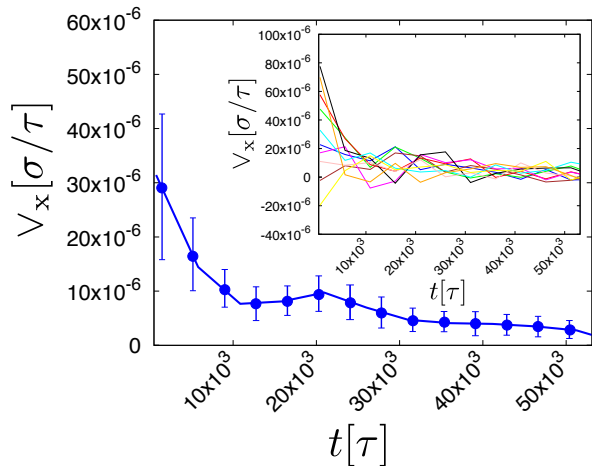


FIG. 8: The instantaneous velocity  $V_x$  of droplets during durotaxis versus elapsed time  $t$  as an average over ten different trajectories ( $V_x(t)$  for individual trajectories is shown in the inset). Here,  $N_p = 600$ ,  $K_0 = 20$ ,  $K' = 2.7$ , and  $\varepsilon_{sp} = 0.7$ .

Eventually, we also analyzed the instantaneous velocity of the droplets for different cases. One of these cases is presented in Fig. 8. It shows that the droplet does not maintain a constant velocity while crossing the substrate along the gradient direction, but rather exhibits faster motion while on the softer part of the substrate. Individual trajectories, however, are seen to fluctuate strongly in their behavior in the course of the process. Overall, the existence of stiffness gradient in the substrate

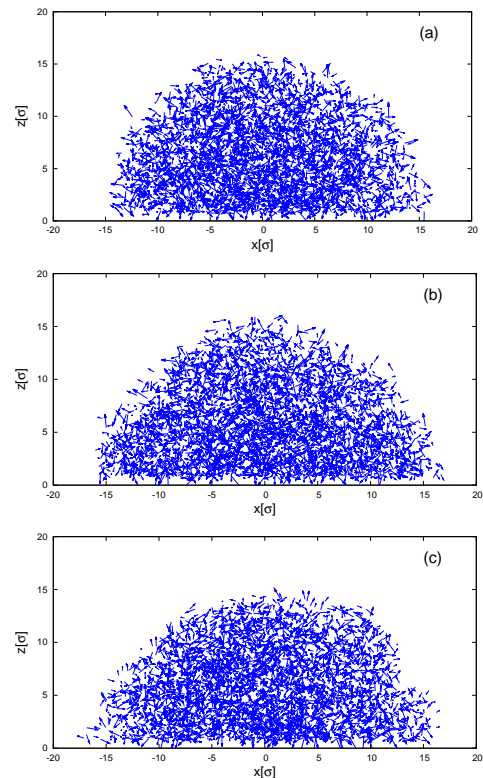


FIG. 9: Typical velocity vector fields in a cross section of the droplet, projected to the  $x - z$  plane, at early (top,  $t = 2.5 \times 10^3 \tau$ ), (middle,  $t = 1.75 \times 10^4 \tau$ ), and late time (bottom,  $t = 4.5 \times 10^4 \tau$ ) during durotaxis for the case of  $N_p = 600$ ,  $K_0 = 20$ ,  $\Delta K = 10.66$ , and  $\varepsilon_{sp} = 0.7$ .

competes with thermal fluctuations, giving rise to a distorted translational movement of droplets to stiffer parts of the substrate. This conclusion is further corroborated by monitoring the velocity field of the droplet at various stages of durotaxis, where no particular pattern for the motion of the polymer chains in the droplet can be readily identified (Fig. 9). In fact, the droplet moves back and forth during durotaxis with the stiffness gradient determining the direction of the motion.

#### IV. CONCLUDING REMARKS

In this study, we have investigated the durotaxis of a droplet onto a substrate, characterized by stiffness gradient in one direction. We observe spontaneous directional movement of the drops from softer to more rigid parts of the substrate, whereby on substrates with equal mean stiffness, durotaxis becomes progressively enhanced upon increasing the stiffness gradient strength. Thereby the average speed of directional motion increases up to a

limiting maximal value. Furthermore, at given stiffness gradient, droplets with better adhesion to the substrate exhibit as a rule essentially faster movement toward the rigid part of the substrate. The latter finding is corroborated by the fact, that smaller droplets are also observed to better wet the substrate [35], owing to a stronger interplay between contact line tension and surface tension of the vapor–polymer melt interface with decreasing size of the drop, exhibiting thus a more efficient durotaxis.

We interpret the observed motion of the droplet towards areas of larger stiffness of the substrate as manifestation of the tendency of the system to acquire energetically favorable states, where the droplet establishes a larger number of contacts between substrate and polymer beads, gaining thus van der Waals contact energy of the droplet particles interaction with the particles of the substrate, in agreement with previous work which considered the durotaxis motion of a flake on a graphene layer [30]. Our computer experiments demonstrate that this

gain in contact energy increases with growing stiffness of the surface.

The present study explores the possibility of guided motion of droplets on variably stiff substrates with implications for nanofluidics, microfabrication, and coating. Our results establish the change in interfacial energy between droplet and substrate as the driving force for durotaxis, and we anticipate that this work will provide further insight into the mechanisms of nanoscale directional motion that has general implications in novel technologies and applications in biology and health care.

This research has been supported by the National Science Centre, Poland, under grant No. 2015/19/P/ST3/03541. This project has received funding from the European Union’s Horizon 2020 research and innovation programme under the Marie Skłodowska–Curie grant agreement No. 665778. This research was supported in part by PLGrid Infrastructure.

- 
- [1] M. Srinivasarao, D. Collings, A. Philips, and S. Patel, *Science* **292**, 79 (2001).
- [2] M. K. Chaudhury and G. M. Whitesides, *Science* **256**, 1539 (1992).
- [3] T.-S. Wong, S. H. Kang, S. K. Y. Tang, E. J. Smythe, B. D. Hatton, A. Grinthal, and J. Aizenberg, *Nature* **477**, 443 (2011).
- [4] G. Lagubeau, M. Le Merrer, C. Clanet, and D. Quéré, *Nat. Phys.* **7**, 395 (2011).
- [5] M. Prakash, D. Quéré, and J. W. Bush, *Science* **320**, 931 (2008).
- [6] A. Darhuber and S. Troian, *Annu. Rev. Fluid Mech.* **37**, 425 (2005).
- [7] H. Gau, S. Herminghaus, P. Lenz, and R. Lipowsky, *Science* **283**, 46 (1999).
- [8] H. Siringhaus, T. Kawase, R. H. Friend, T. Shimoda, M. Inbasekaran, W. Wu, and E. P. Woo, *Science* **290**, 2123 (2000).
- [9] P. Z. Hanakata, B. A. Pazmiño Betancourt, J. F. Douglas, and F. W. Starr, *J. Chem. Phys.* **142** (2015).
- [10] A. Lafuma and D. Quéré, *Nat. Mater.* **2**, 457 (2003).
- [11] L. Courbin, E. Denieul, E. Dressaire, M. Roper, A. Ajdari, and H. A. Stone, *Nat. Mater.* **6**, 661 (2007).
- [12] N. Tretyakov and M. Müller, *Soft matter* **10**, 4373 (2014).
- [13] N. Tretyakov and M. Müller, *Soft Matter* **9**, 3613 (2013).
- [14] G. Karapetsas, N. T. Chamaikos, and A. G. Papathanasiou, *J. Phys.: Condens. Matter* **28**, 085101 (2016).
- [15] D. Dundas, E. J. McEniry, and T. N. Todorov, *Nat. Nanotechnol.* **4**, 99 (2009).
- [16] B. C. Regan, S. Aloni, R. O. Ritchie, U. Dahmen, and A. Zettl, *Nature* **428**, 924 (2004).
- [17] J. Zhao, J.-Q. Huang, F. Wei, and J. Zhu, *Nano Lett.* **10**, 4309 (2010).
- [18] T. Kudernac, N. Ruangsapapichat, M. Parschau, B. Maciá, N. Katsonis, S. R. Harutyunyan, K.-H. Ernst, and B. L. Feringa, *Nature* **479**, 208 (2011).
- [19] O. E. Shklyaev, E. Mockensturm, and V. H. Crespi, *Phys. Rev. Lett.* **110**, 156803 (2013).
- [20] A. M. Fennimore, T. D. Yuzvinsky, W.-Q. Han, M. S. Fuhrer, J. Cumings, and A. Zettl, *Nature* **424**, 408 (2003).
- [21] S. W. D. Bailey, I. Amanatidis, and C. J. Lambert, *Phys. Rev. Lett.* **100**, 256802 (2008).
- [22] A. Barreiro, R. Rurali, E. R. Hernández, J. Moser, T. Pichler, L. Forró, and A. Bachtold, *Science* **320**, 775 (2008).
- [23] H. Somada, K. Hirahara, S. Akita, and Y. Nakayama, *Nano Lett.* **9**, 62 (2009).
- [24] T. Chang and Z. Guo, *Nano Lett.* **10**, 3490 (2010).
- [25] Y. Huang, S. Zhu, and T. Li, *Extreme Mechanics Letters* **1**, 83 (2014).
- [26] M. G. L. van den Heuvel and C. Dekker, *Science* **317**, 333 (2007).
- [27] A. J. Ridley, M. A. Schwartz, K. Burrridge, R. A. Firtel, M. H. Ginsberg, G. Borisy, J. T. Parsons, and A. R. Horwitz, *Science* **302**, 1704 (2003).
- [28] C.-M. Lo, H.-B. Wang, M. Dembo, and Y.-L. Wang, *Biophys. J.* **79**, 144 (2000).
- [29] R. W. Style, Y. Che, S. J. Park, B. M. Weon, J. H. Je, C. Hyland, G. K. German, M. P. Power, L. A. Wilen, J. S. Wettlaufer, et al., *Proc. Natl. Acad. Sci. U.S.A.* **110**, 12541 (2013).
- [30] T. Chang, H. Zhang, Z. Guo, X. Guo, and H. Gao, *Phys. Rev. Lett.* **114**, 015504 (2015).
- [31] J. T. Pham, L. Xue, A. Del Campo, and M. Salierno, *Acta Biomaterialia* **38**, 106 (2016).
- [32] K. A. Lazopoulos and D. Stamenović, *J. Biomech.* **41**, 1289 (2008), ISSN 00219290.
- [33] M. Becton and X. Wang, *RSC Adv.* **6**, 51205 (2016).
- [34] A. S. Barnard, *Nature* **519**, 37 (2015), ISSN 0028-0836.
- [35] P. E. Theodorakis, E. A. Müller, R. V. Craster, and O. K. Matar, *Soft Matter* **11**, 9254 (2015).
- [36] W. Humphrey, A. Dalke, and K. Schulten, *J. Mol. graph.* **14**, 33 (1996).
- [37] K. Kremer and G. S. Grest, *J. Chem. Phys.* **92**, 5057 (1990).
- [38] T. Schneider and E. Stoll, *Phys. Rev. B* **17**, 1302 (1978).
- [39] S. Plimpton, *J. Comp. Phys.* **117**, 1 (1995).

- [40] S. Chen, B. Zhang, X. Gao, Z. Liu, and X. Zhang, *Langmuir* **33**, 24722476 (2017).
- [41] *qhull library used to determine the convex hull of the interfacial area*, URL <http://www.qhull.org>.
- [42] A. I. Milchev and A. A. Milchev, *Europhys. Lett.* **56**, 695 (2001).
- [43] R. D. Gretz, *The Journal of Chemical Physics* **45**, 3160 (1966).